

# Color Transparency at COMPASS<sup>1</sup>

— Feasibility Study —

Andrzej Sandacz<sup>2</sup>, Oleg A. Grajek<sup>2</sup>, Murray Moinester<sup>3</sup>, Eli Piassetzky<sup>3</sup>

<sup>2</sup> Sołtan Institute for Nuclear Studies, ul. Hoża 69, PL 00-681 Warsaw, Poland,

<sup>3</sup> School of Physics and Astronomy, R. and B. Sackler Faculty of Exact Sciences,  
Tel Aviv University, 69978 Ramat Aviv, Israel

*E-mails: sandacz@fuw.edu.pl, oleg@fuw.edu.pl, murraym@tauphy.tau.ac.il,  
eip@tauphy.tau.ac.il*

## Abstract

We examine the potential of the COMPASS experiment at CERN to study color transparency via exclusive vector meson production in hard muon-nucleus scattering. It is demonstrated that COMPASS has high sensitivity to test this important prediction of perturbative QCD.

---

<sup>1</sup> Expanded version of the talk presented at the Workshop on "Nucleon Structure and Meson Spectroscopy" physics to be studied at the COMPASS experiment at CERN, Dubna, Russia, 10–11 October 2000. The conference www site is <http://wwwcompass.cern.ch/compass/workshops/dubna2000/index.html>.

# Contents

<b>1</b>	<b>Introduction</b>	<b>3</b>
<b>2</b>	<b>Experimental method</b>	<b>7</b>
<b>3</b>	<b>Simulation of exclusive <math>\rho^0</math> events</b>	<b>8</b>
3.1	Event generator . . . . .	9
3.2	Simulation of the experimental effects . . . . .	10
<b>4</b>	<b>Results on exclusive <math>\rho^0</math> production</b>	<b>11</b>
<b>5</b>	<b>Comparison with previous experiments</b>	<b>14</b>
<b>6</b>	<b>Open questions</b>	<b>15</b>
<b>7</b>	<b>Conclusions</b>	<b>16</b>
<b>8</b>	<b>Acknowledgements</b>	<b>17</b>

# 1 Introduction

*Color transparency* (CT) is a phenomenon of perturbative QCD (pQCD), whose characteristic feature is that small color-singlet objects interact with hadrons with small cross sections [1, 2, 3, 4]. Cross section for the interaction of such small object, or small size configuration (SSC), with a hadron target has been calculated in QCD using the factorization theorem [5, 4, 6, 7]. These QCD calculations confirmed the hypothesis of F. Low [1] on smallness of the cross section for the interaction of SSC with a hadron, if the gluon density in the hadron is not very high (moderately small  $x$ ). They also predict a related phenomenon of *color opacity* when the gluon density becomes very large (at small  $x$ ) and SSC interacts with the hadron with large cross section [2, 4].

The prerequisite for observing CT is to select a sample containing SSC's via a hard process (i.e. with large  $Q^2$ , high  $p_t$ , or large produced mass). To suppress non-perturbative (not SSC) background different additional restrictions should be imposed depending on the process. For instance for hard exclusive  $\rho^0$  leptonproduction, in addition to large  $Q^2$ , selection of the longitudinally polarized mesons is required. To 'measure' the SSC-nucleon cross sections one should study absorption of the SSC propagating through nuclear matter. In order to clearly observe CT it is necessary that the SSC lives long enough to traverse distances larger than the size of the target nucleus. Another requirement is that SSC stays small while propagating through the nucleus. These requirements, which are quantified in terms of the coherence length and the formation length, are discussed later.

Various processes have been proposed to study CT phenomenon.

- (a) Coherent vector meson ( $J/\psi$ ,  $\rho$ ,  $\phi$ ) production at small  $t$ . For near-forward ( $t \approx 0$ ) coherent production and complete CT, one expects that the cross section for the nuclear target is related to that for the nucleon target by

$$\frac{d\sigma}{dt}(\gamma^* A \rightarrow VA)|_{t \approx 0} = A^2 \frac{d\sigma}{dt}(\gamma^* N \rightarrow VN)|_{t \approx 0}. \quad (1)$$

Gluon shadowing/antishadowing in nuclei is neglected in this formula, but for moderately small  $x (> 0.01)$  this effect is expected to be small. Usually in experiments the  $t$ -integrated coherent cross sections are measured, for which CT predicts an approximate  $A^{4/3}$  dependence. Using more realistic nuclear form factors one predicts  $A^{1.40}$  [8].

Otherwise, if the color-singlet objects, while propagating in nuclear matter, interact with nucleons with large cross sections, the expected  $A$ -dependence is weaker;  $A^{2/3}$  for the cross sections comparable or larger than the pion-nucleon cross section.

- (b) Incoherent (quasi-elastic) vector meson ( $J/\psi$ ,  $\rho$ ,  $\phi$ ) production on nuclei. For complete CT and neglecting effects of the gluon shadowing/antishadowing in the nuclei one expects

$$\frac{d\sigma}{dt}(\gamma^* A \rightarrow VN(A-1)) = A \frac{d\sigma}{dt}(\gamma^* N \rightarrow VN). \quad (2)$$

Here, for the nuclear target the meson  $V$  is produced on a single nucleon of the nucleus and  $(A-1)$  denotes the system of spectator nucleons.

- (c) Coherent or incoherent production of excited vector meson states  $\psi'$  or  $\rho'$ . CT predicts the same  $A$  dependence of  $J/\psi$  and  $\psi'$ , or  $\rho$  and  $\rho'$ . This contrasts with the naive expectations whereby one may expect larger absorption for excited mesons since they are larger.

- (d) Coherent diffractive dissociation of hadrons or photons into high  $p_t$  di-jets. Such process probes the small transverse-size component of the projectile wave-function as well as CT effects. For CT the  $t$ -integrated cross section of coherent diffractive production of high  $p_t$  di-jets has the same  $A$ -dependence as for the processes (a). Using more realistic wave functions one predicts for asymptotically high energies  $A^\alpha$  dependence, where  $\alpha$  is in the range  $1.45 - 1.60$ , depending on  $p_t$  [4].
- (e) Coherent vector meson production on light nuclei (deuteron, helium) in the large  $t$  range, where the effects of double (multiple) scattering are important. CT will suppress the double (multiple) scattering contribution to the differential cross section  $d\sigma/dt$  [4, 9].
- (f)  $A$ -dependence of the fraction of large rapidity gap (diffractive) events. CT predicts an  $A$  independent fraction; otherwise it will grow with  $A$  [10].
- (g) Large  $Q^2$  quasielastic ( $e, e'p$ ) scattering on nuclei,  $eA \rightarrow ep(A - 1)$ . In the CT limit the cross section will be proportional to  $A$ , as for process (b) [11].
- (h) Large  $t$  quasielastic ( $p, 2p$ ) scattering on nuclei,  $pA \rightarrow pp(A - 1)$ . Also for this process, for complete CT the expected  $A$  dependence is like for process (b) [11].

In searches for CT a commonly used quantity, measured in experiments, is the *nuclear transparency*

$$T = \frac{\sigma_A}{A \sigma_N}, \quad (3)$$

which is the ratio of the cross section per nucleon for a selected process on a nucleus  $A$  to the corresponding cross section on a free nucleon. For the incoherent processes CT predicts  $T \simeq 1$  independently of  $A$ . For the large absorption in the nuclear matter  $T$  will be smaller than unity and will decrease with  $A$ . Although the nuclear transparency could be defined also for coherent processes, usually cross sections for coherent production on different nuclei are compared directly. As mentioned above, for  $t$ -integrated coherent cross sections CT predicts  $\sigma_A \propto A^{4/3}$ , whereas for a larger absorption the  $A$ -dependence is weaker.

In the following discussion we concentrate on exclusive vector meson production (VMP), the processes (a)–(c), which could be studied at the COMPASS experiment [12, 13]. Exclusive meson production on the nucleon, free or bound in the nucleus, can be viewed as proceeding according to the diagram shown in Fig. 1. Kinematic variables used in this paper are listed in Table 1.

One of predictions of pQCD is that at high  $Q^2$  the longitudinally polarized virtual photons  $\gamma_L^*$  fluctuate into hadronic components, e.g.  $q\bar{q}$  pairs, whose transverse size  $b = |\bar{r}_{\perp q} - \bar{r}_{\perp \bar{q}}|$  decreases with  $Q^2$ ,  $b \propto (Q^2)^{-1/2}$ . At large  $Q^2$  the values of  $b$  are significantly smaller than the size of the nucleon. For instance, at  $Q^2 = 10 \text{ GeV}^2$  and at  $x = 0.01$   $b_{u\bar{u}} \simeq b_{d\bar{d}} \simeq 0.3 \text{ fm}$  [6], to be compared with the size of  $\rho$  meson  $b_\rho \simeq 1.4 \text{ fm}$ . For transversely polarized photons, in addition to the small size fluctuations, non-perturbative large size components may be expected, even at reasonable large  $Q^2$  ( $\simeq 10 \text{ GeV}^2$ ).

Another pQCD prediction is that the heavy quarks fluctuations, e.g.  $c\bar{c}$ , of the virtual photon have small transverse size already for quasi-real production;  $b_{c\bar{c}} = 0.22 \text{ fm}$  at  $Q^2 \simeq 0$ .

The total cross section for the interaction of a small size  $q\bar{q}$  pair with the nucleon is given in pQCD by the formula [5]

$$\sigma_{q\bar{q}, N} = \frac{\pi^2}{3} b^2 \alpha_s(Q^2) x g(x, Q^2), \quad (4)$$

Table 1: Kinematic variables used in the text.

$k$	four-momentum of the incident muon,
$k'$	four-momentum of the scattered muon,
$p$	four-momentum of the target nucleon,
$v$	four-momentum of the vector meson $V$ ,
$q = k - k'$	four-momentum of the virtual photon,
$-Q^2 = q^2$	invariant mass squared of the virtual photon $\gamma^*$ ,
$\nu = (p \cdot q)/M_p$	energy of the virtual photon in the laboratory system, $M_p$ is the proton mass,
$x = Q^2/(2M_p\nu)$	Bjorken scaling variable,
$y = (p \cdot q)/(p \cdot k)$	fraction of the lepton energy lost in the laboratory system,
$W^2 = (p + q)^2$	total energy squared in the $\gamma^* - N$ system,
$t = (q - v)^2$	four-momentum transfer to the target,
$p_t^2$	transverse-momentum squared of the vector meson with respect to the virtual photon direction,
$m_V = (v^2)^{\frac{1}{2}}$	invariant mass of the vector meson $V$ ,
$M_X^2 = (p + q - v)^2$	missing-mass squared of the undetected recoiled system,
$I = (M_X^2 - M_p^2)/W^2$	inelasticity,
$z = (p \cdot v)/(p \cdot q)$	fraction of the virtual photon energy in the laboratory system taken by meson $V$ ,
	$z \approx 1 - I$

where  $g(x, Q^2)$  is the gluon distribution function in the nucleon. The cross section for the interaction of  $q\bar{q}$  pair of  $b = 0.3$  fm with the nucleon is about 3 mb at  $x = 10^{-2}$  [6]. At very small  $x$  the gluon distribution  $g$  in the nucleon increases, which leads to an increase of the cross section  $\sigma_{q\bar{q}, N}$ . For instance, for  $b = 0.3$  fm  $\sigma_{q\bar{q}, N}$  is about 18 mb at  $x = 10^{-5}$ . Therefore, even for the small  $q\bar{q}$  objects the cross section becomes large at sufficiently small  $x$ . This phenomenon is mentioned earlier *color opacity* and it could be studied at small  $x$  at future electron-nucleus colliders.

In order to study CT for the exclusive production of light quark mesons (like  $\rho$  or  $\rho'$ ) one should select *large*  $Q^2$ , *moderately small*  $x$  and *longitudinally* polarized mesons. For similar studies for the production of  $J/\psi$  or  $\psi'$  one should just select *moderately small*  $x$ .

In studies of CT an important role is played by the *coherence length* and the *formation length*. The coherence length  $l_c$  (sometimes referred to as propagation or interaction length) is defined as the distance traversed by the  $q\bar{q}$  fluctuation of the virtual photon in the target nucleon/nucleus system and is given by

$$l_c = \frac{2\nu}{Q^2 + M^2} = \frac{\beta}{M_N x}. \quad (5)$$

Here  $\beta = Q^2/(Q^2 + M^2)$ ,  $M$  is the invariant mass of the  $q\bar{q}$  fluctuation, and  $M_N$  is the mass of the nucleon. For  $l_c$  values smaller than the size of the nucleus the life-time of the  $q\bar{q}$  fluctuation is short and a chance for the hadronic fluctuation to interact in nuclear matter decreases. In particular this significantly inhibits coherent production. For incoherent production the effects due to the small  $l_c$  values mimic the  $Q^2$  dependence of the nuclear transparency predicted by CT [14].

The formation length is the distance in the target system needed for the  $q\bar{q}$  fluctuation,

which scattered on a nucleon, to develop into a hadron  $h$ . It is equal to

$$l_f = \frac{\nu}{m_h \Delta m}, \quad (6)$$

where  $m_h$  is the mass of the hadron  $h$  and  $\Delta m$  is the mass difference between the hadron  $h$  and its lowest orbital excitation. For small  $l_f$  values the  $q\bar{q}$  fluctuation evolves quickly into a full-size final hadron and the absorption of the final hadron  $h$  in the nucleus plays a role.

Experimentally the effects of the coherence length and the formation length were analysed in detail by the HERMES experiment for incoherent exclusive production of  $\rho^0$  on nuclei [15] and were shown to play an important role at the small  $l_c$  values.

Therefore, for a clean demonstration of CT effects the optimal conditions are when the values of  $l_c$  and  $l_f$  exceed the size of the target nucleus. If the above is not feasible, the variation of nuclear transparency  $T(A, Q^2)$  with  $Q^2$  should be studied for different, fixed values of coherence length. This way, a change of  $T(A)$  between low and high  $Q^2$  values could be associated with the onset of CT, and not with varying  $l_c$ .

The  $t$ -dependence of the cross section for exclusive meson production on the nucleon is approximately exponential,  $e^{b(t-t_{min})}$ , where  $t_{min} \approx -M_p^2 x^2 (1+M^2/Q^2)^2$  and  $M$  is the mass of the produced meson. For soft QCD processes the slope parameter  $b$  should be independent of  $Q^2$ , depending only on the energy. This results from the Regge model [16]. For hard VMP, if SSC's are important, one predicts [17] that the slope  $b$  will significantly decrease with increasing  $Q^2$  approaching a universal value related to the nucleon radius. This is so because the transverse interquark distances in the SSC decrease with increasing  $Q^2$ . This prediction agrees with high energy data on hard diffractive vector meson production on the proton [18, 19, 20].

For VMP on a nucleus  $A$  the  $t$ -dependence of the cross section is approximately reproduced by a sum of two exponential functions. The peak at the lowest  $t$  values, with the slope proportional to the nucleus squared radius  $\langle R_A^2 \rangle$ , is mostly due to the coherent production, whereas at somewhat larger  $t$  the incoherent production on quasi-free nucleons dominates and the slope is equal to that for the production on free nucleons. Applying cuts on  $t$  allows to select samples of events, which are strongly dominated by either coherent or incoherent production. It was successfully demonstrated in Refs [8, 23, 26].

In order to observe maximal coherent exclusive meson production for which the whole nucleus contributes, it is necessary to satisfy the condition

$$|t_{min} \langle R_A^2 \rangle / 3| \ll 1. \quad (7)$$

In the COMPASS experiment for low  $x$  values in the range 0.006 – 0.02 and for  $Q^2 \approx 2 - 10 \text{ GeV}^2$ , one has  $|t_{min} \langle R_A^2 \rangle / 3| \approx 10x^2 A^{2/3}$  and the condition (7) is satisfied even for lead ( $A = 207$ ).

Experimental searches for CT started more than a decade ago and encompass various processes: large  $t$  quasielastic ( $p, 2p$ ) scattering [21], large  $Q^2$  quasielastic ( $e, e'p$ ) scattering [22],  $J/\psi$  photoproduction [8] and  $J/\psi$  muoproduction [23], exclusive  $\rho^0$  leptonproduction [24, 25, 15] and coherent diffractive dissociation of the pion into two high- $p_t$  jets [26].

The pioneering studies of CT in large  $t$  quasi-elastic proton scattering [21] found a rise of the nuclear transparency as the beam energy increased from 6 to 9 GeV and a decrease at higher energies. The large  $Q^2$  quasi-elastic electron scattering studies [22] did not show  $Q^2$  dependence. The explanation of these results in terms of CT is still debatable.

Strong recent evidence for CT comes from Fermilab E791 experiment on the  $A$ -dependence of coherent diffractive dissociation of pions into two high- $p_t$  jets [26]. Also the

E691 results on  $A$ -dependence of coherent  $J/\psi$  photoproduction [8] and the NMC measurements of  $A$ -dependence of coherent and quasielastic  $J/\psi$  muoproduction are consistent with CT. Measurements of the nuclear transparency for incoherent exclusive  $\rho^0$  production by Fermilab experiment E665 give a hint for CT. However, due to the low statistics of that data at high  $Q^2$ , it was not possible to disentangle effects of decreasing  $l_c$  at high  $Q^2$  and to demonstrate CT unambiguously.

## 2 Experimental method

We propose to study CT via *exclusive vector meson production*  $\mu A \rightarrow \mu V A$  (coherent) and  $\mu A \rightarrow \mu V N(A-1)$  (incoherent) on various nuclei  $A$  and optionally also on a proton or deuteron target. As a primary objective we propose to study the production of the following mesons  $V$ :  $\rho^0$ ,  $J/\psi$ ,  $\phi$ ,  $\psi'$  ( $\psi(2S)$ ) and  $\rho'$  ( $\rho(1450)$ ,  $\rho(1700)$ ). Also investigations of the production of other mesons will be possible. The preferable decay modes are those into the charged particles:  $\rho^0 \rightarrow \pi^+\pi^-$ ,  $J/\psi \rightarrow e^+e^-/\mu^+\mu^-$ ,  $\phi \rightarrow K^+K^-$ ,  $\psi' \rightarrow J/\psi \pi^+\pi^-$ ,  $\rho' \rightarrow \pi^+\pi^+\pi^-\pi^-$ . Two or more nuclear targets will be used. An additional proton (deuteron) target would be beneficial.

Our proposal is to complement the initial setup of the COMPASS [12, 13] for the muon run with the polarized target, by adding two thin nuclear targets of lead and carbon of 17.6 g/cm<sup>2</sup> each. The carbon target will be a cylinder 8 cm long and of 3 cm of diameter. The lead target will consist of 4 discs of 3 cm of diameter, distributed over length of 8 cm. Only one nuclear target will be exposed to the muon beam at a time, with frequent exchanges (every few hours) of different targets. The nuclear targets will be located downstream of the polarized target, at the end of the solenoid magnet and before the first tracking detector (first micromega chamber).

The high-intensity high-energy incident muon-beam will impinge on the polarized target and a downstream thin nuclear target. The momenta of the scattered muon and of the produced charged particles will be reconstructed in the two magnetic spectrometers, using the magnets SM1 and SM2, instrumented with micromega chambers, drift chambers, GEM detectors, straw chambers, multiwire proportional chambers and scintillating fibers. Adding a recoil detector which will surround the nuclear target and register slow particles emitted from it may not be possible for the present setup due to the limited space. However, it would be advantageous and possible for dedicated runs taken with a modified setup. In the following we assume that the recoil particle(s) remain(s) undetected, and in order to select exclusive events one has to rely only on the kinematics of the scattered muon and the produced meson.

The trigger will use the information from hodoscopes registering the scattered muons, and from calorimeters registering deposits of energy of the particles in the final state. For VMP reactions triggering only on the scattered muon is in principle possible. However, for better efficiency of the trigger, especially at small  $Q^2$ , it will be useful for certain processes to require in addition a minimum energy deposit in the calorimeters.

The off-line selection of exclusive events for the production of different mesons will be similar to that described for  $\rho^0$  production in Ref. [25, 27, 28]. In particular the discrimination of non-exclusive events will be done by applying cuts on the inelasticity  $I$  (for the definition see Table 1). In Fig. 2 the inelasticity distribution is shown for the SMC  $\rho^0$  sample [29] for the events with the invariant mass in the central part of the  $\rho^0$  peak. For the inelasticity distribution the peak at  $I = 0$  is the signal of exclusive  $\rho^0$  production.

Non-exclusive events, where in addition to detected fast hadrons, slow undetected hadrons were produced, appear at  $I > 0$ . For the cut  $-0.05 < I < 0.05$  defining the exclusive sample the amount of the residual non-exclusive background for the SMC experiment was up to about 10% at large  $Q^2$ . The kinematical smearing in  $I$  and the width of the elastic peak in COMPASS is expected to be about the same (cf. Sect. 3.2) as that shown in Fig. 2 for the SMC experiment. Although the smearing will be similar, we expect the level of the non-exclusive background to be lower in COMPASS due to the wider angular and momentum acceptance coverage for final state hadrons. In addition, with larger statistic in COMPASS it will be possible to apply more tight inelasticity cuts, further reducing the background. The effect of this residual background on various observables will be studied by varying the inelasticity cuts, similarly as was done in Ref. [30].

The selections of coherent or incoherent production will be done on a statistical basis, using the  $t$ -distribution; at the lowest  $|t|$  values coherent events predominate, whereas at somewhat larger  $|t|$  there is almost clean sample of incoherent events.

Separation of the  $\rho^0$  samples with the enhanced content of longitudinally or transversely polarized mesons will be done by applying cuts on the measured angular distributions of pions from the decays of the parent  $\rho^0$ .

The minimal covered  $Q^2$  range is expected to be  $0.05 < Q^2 < 10 \text{ GeV}^2$ . For the medium and large  $Q^2$  values ( $Q^2 > 2 \text{ GeV}^2$ ) the range  $0.006 < x < 0.1$  will be covered with good acceptance.

The basic observable for each process studied will be the ratio of the nuclear transparencies for lead and carbon,  $R_T = T_{\text{Pb}}/T_{\text{C}} = (\sigma_{\text{Pb}}/A_{\text{Pb}})/(\sigma_{\text{C}}/A_{\text{C}})$ . Due to the proposed geometry of the targets, the acceptances will cancel in the ratio  $R_T$ . Also the absolute beam flux measurement will not be necessary for the ratio  $R_T$ , provided that the relative determination of the beam fluxes for the exposures with different target materials could be done, e.g. by counting DIS events originating in the polarized target. The measured ratio  $R_T$  should be corrected for different losses of events in lead and carbon, which are due to the secondary interactions in the targets. They will be estimated from the MC simulations.

### 3 Simulation of exclusive $\rho^0$ events

In this section we describe details of the simulation of exclusive coherent ( $\mu A \rightarrow \mu \rho^0 A$ ) and incoherent ( $\mu A \rightarrow \mu \rho^0 N(A-1)$ )  $\rho^0$  production in the COMPASS experiment with the carbon and lead targets. The simulations were done with a dedicated fast Monte Carlo program which generates deep inelastic exclusive  $\rho^0$  events with subsequent decay  $\rho^0 \rightarrow \pi^+ \pi^-$ . At this stage there was no attempt to include any background in the event generators. Here we describe the event generator as well as the treatment of different experimental aspects: losses due to the secondary interactions of pions, propagation through the magnetic fields, angular and momentum resolutions, muon trigger acceptance, acceptance for final state pions and efficiency of tracks reconstruction.

Radiative corrections for exclusive  $\rho^0$  production are expected to be similar to those for the NMC experiment, which were in the range of 2% to 5% [31]. These corrections were not included in the present simulations.



### 3.1 Event generator

First we present the used parameterization of the cross section for the production on the free nucleon,  $\mu N \rightarrow \mu \rho^0 N$ , with the subsequent decay  $\rho^0 \rightarrow \pi^+ \pi^-$ :

$$\sigma_{\mu N \rightarrow \mu \rho^0 N} = \Gamma_T(Q^2, \nu) \cdot \sigma_{\gamma^* N \rightarrow \rho^0 N}^{\text{tot}}(Q^2, \nu) \cdot F(p_t^2, \cos \theta, \phi), \quad (8)$$

where  $\theta$  and  $\phi$  are, respectively, the polar and azimuthal angles of  $\pi^+$  from the decay, calculated in the parent  $\rho^0$  center-of-mass system, with respect to the direction of flight of  $\rho^0$ ,  $\Gamma_T$  is the flux of transverse virtual photons

$$\Gamma_T = \frac{\alpha(\nu - \frac{Q^2}{2M_p})}{2\pi Q^2 E_\mu^2 (1 - \epsilon)}, \quad (9)$$

$\alpha$  is the fine-structure constant,  $E_\mu$  the muon-beam energy and  $\epsilon$  is the virtual photon polarization given by

$$\epsilon = \frac{1 - \frac{\nu}{E_\mu} - \frac{Q^2}{4E_\mu^2}}{1 - \frac{\nu}{E_\mu} + \frac{1}{2}\left(\frac{\nu}{E_\mu}\right)^2 + \frac{Q^2}{4E_\mu^2}}. \quad (10)$$

The virtual photon cross section was parametrized as

$$\sigma_{\gamma^* N \rightarrow \rho^0 N}^{\text{tot}}(Q^2, \nu) = 27.4 \text{ nb} \cdot \left( \frac{6 \text{ GeV}^2}{Q^2} \right)^{1.96}. \quad (11)$$

This is the NMC parametrisation of the cross sections per nucleon for exclusive  $\rho^0$  production on carbon [25]. As the NMC data shows little  $A$ -dependence of the virtual photon ( $t$ -integrated) cross section per nucleon, we use the same parametrisation of  $\sigma_{\gamma^* N \rightarrow \rho^0 N}^{\text{tot}}$  for carbon and proton targets. This parametrisation does not apply at small  $Q^2$  values, namely at  $Q^2 < 1 \text{ GeV}^2$ .

The function  $F$  comprises the  $p_t^2$  distributions of produced  $\rho^0$  and the angular distributions of pions coming from its decay

$$F = a_L \cdot f_L(p_t^2) \cdot W_L(\cos \theta, \phi) + a_T \cdot f_T(p_t^2) \cdot W_T(\cos \theta, \phi). \quad (12)$$

Here  $a_L = r_{00}^{04}$ ,  $a_T = 1 - r_{00}^{04}$ ,  $r_{00}^{04} = r_{00}^{04}(Q^2, \nu)$  is the  $\rho^0$  density matrix element, which can be identified as a fraction of longitudinally polarized (helicity = 0)  $\rho^0$  mesons, and the indices  $L$  and  $T$  refer to longitudinally and transversely polarized  $\rho^0$ 's, respectively. The fraction  $r_{00}^{04}$  can be expressed [32] by the ratio  $R$  of the cross sections for exclusive production by longitudinal and transverse virtual photons. We use a parametrisation of  $R$  given by [33] which reproduce data on exclusive  $\rho^0$  production in a wide range of  $Q^2$ .

The  $p_t^2$  distributions are described by

$$f_i(p_t^2) = b_i e^{-b_i p_t^2}, \quad (13)$$

where  $i = L$  or  $T$ ,  $b_L = 4.5 + 4 \cdot (0.5/Q^2) \text{ GeV}^{-2}$  and  $b_T = 8.5 \text{ GeV}^{-2}$ . These parameterizations weighted by the fractions of longitudinally and transversely polarized mesons allow to reproduce reasonably the values of the effective slope  $b$  for the exclusive  $\rho^0$  production measured at HERA and in the fixed-target experiments in a wide range of  $Q^2$ .

The angular distributions of the pions from  $\rho^0$ 's decays are given by

$$W_i(\cos \theta, \phi) = \frac{1}{2\pi} \frac{3}{4} \left\{ (1 - P_i) + (3P_i - 1) \cos^2 \theta \right\}, \quad (14)$$

where  $i = L$  or  $T$ ,  $P_L = 0$  and  $P_T = 1$ . For the nuclear targets we assume the same  $W_i$  distributions as for the proton as suggested by [25]. Note that the distributions  $f_i(p_i^2)$ ,  $W_i(\cos\theta, \phi)$  and  $F(p_i^2, \cos\theta, \phi)$  are normalized to unity.

The invariant mass of two decay pions was generated using the relativistic p-wave Breit-Wigner shape for the  $\rho$  resonance [34].

We relate the differential cross sections for the proton

$$\left(\frac{d\sigma_N}{dt}\right)_i \equiv \Gamma_T \cdot \sigma_{\gamma^* N \rightarrow \rho^0 N}^{\text{tot}} \cdot a_i \cdot f_i(-t), \quad (15)$$

to these for coherent and incoherent production on the nucleus  $A$  by

$$\left(\frac{d\sigma_A^{\text{coh}}}{dt}\right)_i = A_{\text{eff, coh}}^2 \cdot e^{\langle R_A^2 \rangle t/3} \cdot \left(\frac{d\sigma_N}{dt}\right)_i, \quad (16)$$

$$\left(\frac{d\sigma_A^{\text{inc}}}{dt}\right)_i = A_{\text{eff, inc}} \cdot \left(\frac{d\sigma_N}{dt}\right)_i, \quad (17)$$

respectively. Here  $\langle R_A^2 \rangle$  is the mean squared radius of the nucleus,  $A_{\text{eff, coh}}$  and  $A_{\text{eff, inc}}$  take account of nuclear screening for the coherent and incoherent processes, correspondingly. The cross section for incoherent exclusive meson production is summed over all final states of the recoiling system, i.e. it is given for the so called closure approximation. The suppression of the incoherent cross section at small  $t$  due to the Pauli blocking is neglected here. We used the approximation  $t - t_{\text{min}} \simeq -p_t^2$ , where  $|t_{\text{min}}|$  is the minimal kinematically allowed  $|t|$  value for given  $W^2$ ,  $Q^2$ ,  $m_V$  and  $M_X^2$ .

We generated the cross sections for two models. For the complete color transparency model (CT model) we used  $A_{\text{eff, coh}} = A_{\text{eff, inc}} = A$ . In another model we assumed a substantial nuclear absorption (NA model) and used  $A_{\text{eff, coh}} = A_{\text{eff, inc}} = A^{0.75}$ . These could be compared to different predictions of the vector meson dominance model (VMD), which vary depending on the  $\rho$  meson-nucleon total cross section and on the coherence length  $l_c$  (see e.g. [35]). The  $A$  dependences of the NA model are in the range of predictions of VMD, except for incoherent production at large  $l_c$ , where VMD predicts stronger nuclear absorption.

### 3.2 Simulation of the experimental effects

The secondary hadronic interactions of the decay pions in the target were simulated. The assumed density of targets,  $\rho_{\text{tgt}}$ , was 2.2 g/cm<sup>3</sup>. The interaction length  $\lambda_{\text{int}}^\pi$  for pions in the target material, was assumed equal to 130 g/cm<sup>2</sup> for the carbon and 290 g/cm<sup>2</sup> for the lead target. For an exclusive  $\rho^0$  event to be reconstructible, it was required that none of the decay pions underwent an inelastic hadronic interaction.

The trajectories of charged particles were simulated taking into account the geometry of SM1 and SM2 magnets of the COMPASS experiment. Homogeneous fields inside both magnets were assumed. For the SM1 magnet the bending power  $\int B dl$  was assumed equal to 1.0 T·m (independent of the beam energy), whereas for the SM2 magnet it was assumed equal to 2.3 T·m for a 100 GeV muon beam energy, and 5.2 T·m for a 190 GeV muon beam. After tracking of the produced charged particles through the detector, a flag was assigned to each particle telling how far it propagated in the COMPASS setup.

Kinematic smearing of the beam, of the scattered muon and of the charged hadrons was simulated. Assumed values of dispersions of measured particle momenta and angles are

based on the experience of previous muon experiments at CERN, as well as on the results of studies at COMPASS. The relative error on the momentum,  $\sigma(p)/p$ , was assumed equal to 0.5% for beam tracks, 0.75% for the tracks passing only the first magnet and 0.44% for the tracks passing the second magnet. The error on the angle of a particle was assumed to be 0.15 mrad. For a 190 GeV beam and the kinematic cuts listed in Section 3 the resulting smearing of the inelasticity  $I$  is about 0.018 and the smearing of the invariant mass of two pions is about 6 MeV.

To simulate the trigger acceptance a trajectory of the scattered muon behind the second magnet was calculated, and the hits in the muon hodoscopes H4 and H5 were checked. Each of these two hodoscopes consists in fact of a few different hodoscopes (namely of the Ladders, the Primed System, the Unprimed System) but for the purpose of the present analysis we will consider just two cases, corresponding to different trigger acceptances. First, we assumed that only the Ladders and the Primed System are available. This trigger is called the Medium  $Q^2$  range Trigger (MT). If in addition the Unprimed System is also implemented, the Full  $Q^2$  range Trigger (FT) will result. The  $Q^2$  dependence of the trigger efficiency,  $\epsilon_{\text{tr}}$ , for these triggers was presented in [27]. For the MT trigger at 190 GeV beam  $\epsilon_{\text{tr}}$  decreases quickly with  $Q^2$  from 0.7 at  $Q^2 = 2 \text{ GeV}^2$  to about 0.1 at  $Q^2 = 10 \text{ GeV}^2$ . The acceptance is several times smaller for this trigger at 100 GeV beam. For the FT trigger the  $Q^2$  dependence is weaker and the trigger acceptance is higher; it is always bigger than 0.5 for  $Q^2 < 70 \text{ GeV}^2$  at 190 GeV beam energy and for  $Q^2 < 20 \text{ GeV}^2$  at 100 GeV beam. In conclusion, for the MT trigger the data taking with the higher beam energy seems the only acceptable choice, whereas for the FT trigger running at both beam energies is feasible, although the covered  $Q^2$  range is larger at the higher beam energy.

For a  $\rho^0$  meson to be accepted it was required that each pion from its decay was emitted in the laboratory at an angle within the acceptance of the SM1 magnet, and that its momentum was bigger than 2 GeV.

Based on the preliminary results of the track reconstruction by the programs developed at COMPASS, simple and rather conservative assumptions were used to simulate the efficiency of tracks reconstruction. For the tracks seen only in the first spectrometer the single track reconstruction efficiency was assumed equal to 0.8 for the momentum range  $p > 2 \text{ GeV}$ , and for the tracks observed also in the second spectrometer it was assumed equal to 0.95. The efficiency  $\epsilon_{\text{rec}}$  to reconstruct all three tracks of the scattered muon and of two pions was assumed to be equal  $0.7 \cdot 0.95^3 + 0.3 \cdot 0.95^2 \cdot 0.80$ . This assumption was motivated by the observation that for 70% of accepted DIS exclusive  $\rho^0$  events all three measured tracks are seen in the second spectrometer, while for the remaining 30% events the scattered muon and the fast pion are seen in both first and second spectrometers, whereas the slow pion is observed in the first spectrometer only.

## 4 Results on exclusive $\rho^0$ production

Due to the higher trigger efficiency and larger  $Q^2$  range at higher beam energy we considered 190 GeV muon beam. The simulations were done independently for the carbon ( $A = 12$ ) and lead targets ( $A = 207$ ), and for two triggers (MT and FT). For each target and each trigger we assumed two different models describing the nuclear effects for exclusive  $\rho^0$  production: CT model and NA model (cf. Section 3.1).

The kinematic range considered was the following:

$$2 < Q^2 < 80 \text{ GeV}^2, \quad (18)$$

Table 2: Numbers of accepted events for two considered models of the nuclear absorption.

model	$N_C$	$N_{Pb}$
CT	70 000	200 000
NA	28 000	20 000

$$35 < \nu < 170 \text{ GeV} . \quad (19)$$

The upper cut on  $\nu$  was chosen to eliminate the kinematic region where the amount of radiative events is large, whereas the lower one to eliminate the region where the acceptance for pions from  $\rho^0$  decay is low.

The total efficiency  $\epsilon_{\text{tot}}$  to observe exclusive  $\rho^0$  events results from: the acceptance of the trigger ( $\epsilon_{\text{tr}}$ ), acceptance to detect the pions ( $\epsilon_{\text{had}}$ ), efficiency for tracks reconstruction ( $\epsilon_{\text{rec}}$ ), cut on the invariant mass of two pions,  $0.62 < M_{\pi\pi} < 0.92 \text{ GeV}^2$ , used for the selection of the samples ( $\epsilon_{\text{mass}}$ ), and efficiency for an event to survive the secondary interactions ( $\epsilon_{\text{sec}}$ ). The contributions of all these effects to  $\epsilon_{\text{tot}}$  are similar to those presented in [27] for the polarized target, except for the effects of the secondary interactions. The approximate value of  $\epsilon_{\text{sec}}$  is equal to 0.87 for the carbon target and 0.94 for the lead target. The total efficiency  $\epsilon_{\text{tot}}$  is about 0.48 for the FT trigger and about 0.30 for the MT trigger.

The total expected cross section for exclusive  $\rho^0$  production on the nucleon is

$$\sigma_{\mu N \rightarrow \mu \rho^0 N}^{\text{tot}} = \int_{\nu_{\text{min}}}^{\nu_{\text{max}}} \int_{Q_{\text{min}}^2}^{Q_{\text{max}}^2} \sigma_{\mu N \rightarrow \mu \rho^0 N}(Q^2, \nu) dQ^2 d\nu , \quad (20)$$

where the kinematic range was defined before. The value of  $\sigma_{\mu N \rightarrow \mu \rho^0 N}^{\text{tot}}$  is 283 pb. For nuclear targets the corresponding values depend on  $A$  and on the assumed model for nuclear absorption.

The expected muon beam intensity will be about  $10^8/\text{s}$  during spills of length of about 2 s, which will repeat every 14.4 s. With the proposed thin nuclear targets, each of  $17.6 \text{ g/cm}^2$ , the luminosity will be  $\mathcal{L} = 12.6 \text{ pb}^{-1} \cdot \text{day}^{-1}$ . The estimates of the numbers of accepted events were done for a period of data taking of 150 days (1 year), divided equally between two targets. An overall SPS and COMPASS efficiency of 25% was assumed. The numbers of accepted events for the carbon and lead targets, assuming the two models for the nuclear absorption mentioned earlier, are given in Table 2.

The distributions of accepted exclusive events as a function of  $x$ ,  $Q^2$  and  $\nu$  are similar to those presented in [27].

In Fig. 3 we present the  $p_t^2$  distributions for both targets. We observe clear coherent peaks at small  $p_t^2$  ( $< 0.05 \text{ GeV}^2$ ) and less steep distributions for the incoherent events at larger  $p_t^2$ . The arrows at the top histograms indicate the cut  $p_t^2 > 0.1 \text{ GeV}^2$ , used to select the incoherent samples. The contribution from coherent events is negligible in these samples. For the middle and bottom histograms the arrows indicate the cut  $p_t^2 < 0.02 \text{ GeV}^2$ , used to select the samples which are dominated by coherent events — the so called coherent samples. For the samples defined by the latter cut the fraction of the incoherent events is at the level of up to 10%, depending on the nucleus and on the model for nuclear absorption. We plan also to use the standard method to determine coherent and incoherent components, by fitting  $p_t^2$  distribution.

The effect of the kinematical smearing on  $p_t^2$  may be seen by comparing the distributions for the generated events (middle row) to the ones for measured events (bottom row) where the acceptance and smearing were included. The smearing of  $p_t^2$  increases with increasing  $p_t^2$ ; it is about  $0.006 \text{ GeV}^2$  for the coherent samples ( $p_t^2 < 0.02 \text{ GeV}^2$ ) and about  $0.03 \text{ GeV}^2$  for the incoherent samples ( $p_t^2 > 0.1 \text{ GeV}^2$ ).

The analysis of the  $\rho$  decay distributions allows us to study spin-dependent properties of the production process [32], in particular the polarization of  $\rho$ . Usually the  $\rho^0$  decay angular distribution  $W(\cos\theta, \phi)$  is studied in the  $s$ -channel helicity frame, which is the most convenient for describing the  $\rho$  decay after photo- and electroproduction [36]. The  $\rho^0$  direction in the virtual photon-nucleon centre-of-mass system is taken as the quantization axis. The angle  $\theta$  is the polar angle and  $\phi$  the azimuthal angle of the  $\pi^+$  in the  $\rho^0$  centre-of-mass system. The  $\cos\theta$  distributions for pions from  $\rho^0$  decays are shown in Fig. 4 for the lead target. The distributions for longitudinally (dashed lines) and transversely (dotted lines) polarized parent  $\rho^0$ 's are markedly different. Their sum is also indicated.

Usually fits to the combined  $\cos\theta$  distributions are performed in order to determine the density matrix element  $r_{00}^{04}$  (cf. Eq. 11), which can be identified as the probability that the  $\rho^0$  was longitudinally polarized. For exclusive  $\rho^0$  production the approximate  $s$ -channel helicity conservation (SCHC) is observed [37, 18], i.e. the helicity of  $\rho^0$  is predominantly equal to that of the virtual photon. Assuming SCHC and using the fitted  $r_{00}^{04}$  one can estimate the ratio  $R = \sigma_L/\sigma_T$  for exclusive virtual photoproduction ([32]). In COMPASS we plan to measure  $R$  as well, and study its  $Q^2$ - and  $A$ -dependence, which is expected to reflect the strength of nuclear absorption.

As  $Q^2$  increases, the approach to the CT limit is expected to be different for VMP by longitudinally polarized virtual photons from that by transversely polarized photons. Therefore, in order to increase the sensitivity of the search for CT, we propose another method. It consists in studying  $A$ -dependence of the cross sections for samples with different  $\rho^0$  polarizations, which will be selected by cuts on  $\cos\theta$ . For instance, after applying the cut  $|\cos\theta| > 0.7$  the fraction of accepted events with  $\rho_L^0$  is (80–95)% depending on the simulation, whereas for the cut  $|\cos\theta| < 0.4$  the fraction of events with  $\rho_T^0$  is (75–92)%. For an approximate SCHC, such cuts will allow us to select the samples with enhanced contributions of the events initiated by the virtual photons of a desired polarization. Studies of the samples with *different polarizations* of the virtual photons are *important* for the clear demonstration of CT.

Another aspect which is important for CT studies, is the covered range of the coherence length  $l_c$  (cf. Section 1). In Fig. 5 we present the plot of  $l_c$  vs.  $Q^2$  for a sample of accepted events. The effects of initial and final state interactions in the nuclei vary at small  $l_c$  values [15]. Therefore, it was suggested that in order to disentangle effects due to CT from those caused by the modified absorption at small  $l_c$  values, one should study  $A$ - and  $Q^2$ -dependences of cross sections at fixed values of  $l_c$ . This approach will be possible, if large statistics data were available.

For a limited statistics, a possible solution to avoid the mentioned effects is to use the combined data at  $l_c$  values exceeding the sizes of the target nuclei. The radius of the carbon nucleus is  $\langle r_C^2 \rangle^{1/2} = 2.5 \text{ fm}$  and that of the lead nucleus is  $\langle r_{Pb}^2 \rangle^{1/2} = 5.5 \text{ fm}$  [38]. Therefore, one may use the selection  $l_c > l_c^{\min} \simeq 2 \cdot \langle r_{Pb}^2 \rangle^{1/2} = 11 \text{ fm}$ . The value of  $l_c^{\min}$  is indicated in Fig. 5 by arrows. About a half of events survive the cut on  $l_c$ . These events cover the range of  $Q^2 < 6 \text{ GeV}^2$ , which is expected to be sufficient to observe CT.

The estimated values and statistical precision of  $R_T$ , the ratio of the nuclear transparencies for lead and carbon, are presented for different  $Q^2$  bins in Fig. 6 for  $p_t^2 < 0.02 \text{ GeV}^2$

Table 3:  $Q^2$  bins used for the determination of  $R_T$ .

Bin number	$Q^2$ bin [GeV <sup>2</sup> ]	$\langle Q^2 \rangle$ [GeV <sup>2</sup> ]	$\langle x \rangle$
1	2–3	2.4	0.016
2	3–4	3.4	0.022
3	4–6	4.8	0.031
4	6–9	7.2	0.048
5	9–12	10.2	0.072
6	12–20	14.8	0.11

and in Fig. 7 for  $p_t^2 > 0.1 \text{ GeV}^2$ . The  $Q^2$  bins are specified in Table 3. Each figure comprises predictions for two models, CT and NA, and for 6 different samples of accepted events for each model. For each sample a set of "measurements" in different  $Q^2$  bins is shown. Sets **A** and **B** were obtained using the standard selections for the MT and FT triggers, respectively. Four remaining sets were obtained for the FT trigger with additional selections: **C** with  $|\cos\theta| < 0.4$ , **D** with  $|\cos\theta| > 0.7$ , **E** with  $|\cos\theta| < 0.4$  and  $l_c > 11 \text{ fm}$ , and **F** with  $|\cos\theta| > 0.7$  and  $l_c > 11 \text{ fm}$ . Note that for sets **E** and **F** only three lower  $Q^2$  bins appear (cf. Fig. 5). One expects large differences in  $R_T$  for the two considered models. For coherent samples  $R_T \approx 5$  for CT model and  $\approx 1$  for NA model. At  $Q^2 \simeq 5 \text{ GeV}^2$  the precision of the measurement of  $R_T$  for coherent events will be better than 17%, even for the restricted samples **E** and **F**, thus allowing excellent discrimination between the two models for the nuclear absorption. For the incoherent events the power to discriminate models by  $R_T$  measurements will be more limited.

## 5 Comparison with previous experiments

In this section we compare COMPASS capabilities to demonstrate CT to those of previous experiments in which exclusive  $\rho^0$  leptonproduction on nuclear targets was studied. We concentrate on this reaction, as among different exclusive VMD channels it has the largest cross section. For the comparison we have selected experiments which covered  $Q^2$  range extending to large values, bigger than  $2 \text{ GeV}^2$ . This condition is satisfied for the following experiments: HERMES [15], NMC [25] and E665 [24].

The published results from the HERMES experiment concern the incoherent exclusive  $\rho^0$  production on  $^1\text{H}$ ,  $^2\text{H}$ ,  $^3\text{He}$  and  $^{14}\text{N}$  targets. The electron beam energy was  $27.5 \text{ GeV}$  and the covered  $Q^2$  and  $l_c$  ranges are  $0.4 < Q^2 < 5.5 \text{ GeV}^2$  and  $0.6 < l_c < 8 \text{ fm}$ . Like in all fixed-target experiments with lepton beams, the covered kinematic range is such that for a given  $Q^2$  the average value of  $l_c$  decreases with increasing  $Q^2$ . The highest values of the HERMES data where one may expect to observe the onset of CT are correlated with the small values of  $l_c$  below  $2 \text{ fm}$ . The increase of the nuclear transparency observed for  $^{14}\text{N}$  is explained as due to the reduced coherence length, without resorting to CT.

Wider kinematic ranges were covered by experiments using high-energy muon beams. NMC has published the data on coherent and incoherent exclusive  $\rho^0$  production on  $^2\text{H}$ , C and Ca targets. The muon beam energy was 200 GeV and the data cover the ranges  $2 < Q^2 < 25 \text{ GeV}^2$  and  $1 < l_c < 30 \text{ fm}$ . For the NMC kinematic range, the large values of  $l_c$  which exceed the diameter of the largest target nucleus (Ca),  $l_c > 7 \text{ fm}$ , correspond to  $Q^2 < 5.5 \text{ GeV}^2$ . In principle, in this range it is possible to study  $Q^2$  dependence of nuclear absorption in order to observe CT not obscured by effects of small  $l_c$ . However, due to the moderate statistics of the data, such detailed analysis was not possible for NMC.

The most favourable kinematical conditions were realised in the E665 experiment due to the high muon beam energy of 470 GeV. The experiment has published the data on incoherent exclusive  $\rho^0$  production on  $^1\text{H}$ ,  $^2\text{H}$ , C, Ca and Pb targets. The data were taken in a wide  $Q^2$  range, including also very small values  $Q^2 > 0.1 \text{ GeV}^2$ , and in a wide range of  $l_c$ ,  $1 < l_c < 200 \text{ fm}$ . At small and moderate  $Q^2$  values,  $< 3 \text{ GeV}^2$ , which correlate with  $l_c$  values exceeding the diameter of the lead nucleus, precise measurements of the nuclear transparency were obtained. They indicate strong nuclear absorption. At the highest  $Q^2$  bin,  $Q^2 > 3 \text{ GeV}^2$ , the nuclear transparency increases in qualitative agreement with CT. However, the data in this bin correspond to a wide range of  $l_c$ ,  $1 < l_c < 40 \text{ fm}$ , and therefore could be affected by effects due to the reduced coherence length. The low statistics in the large  $Q^2$  bin did not allow more detailed studies.

The COMPASS data at medium and large  $Q^2$  (FT trigger) will cover the kinematic range similar to that of the NMC data. The expected statistics for the carbon target will be about 2 orders of magnitude higher than that of the NMC data for the same target. This increase is in particular due to higher beam intensity and larger acceptance in the COMPASS experiment. Similarly like in the E665 experiment COMPASS will use also lead target and will extend measurements to small  $Q^2$ . The statistics of COMPASS data will be significantly higher also than that of E665. For example, for incoherent events at  $Q^2 > 3 \text{ GeV}^2$  the ratio of nuclear transparencies for lead and carbon will be determined with accuracy better than 3%, comparing to about 30% for E665. Another more sensitive method to study nuclear effects in exclusive  $\rho^0$  production, the one by using coherent production, will be employed in COMPASS as well. Due to large statistics splitting of COMPASS data in several  $Q^2$  and  $l_c$  bins as well as the selection of events with longitudinal or transverse  $\rho^0$  polarization will be possible.

## 6 Open questions

In addition to the  $\rho^0$  production, we will study exclusive production of  $J/\psi$ ,  $\phi$ ,  $\psi'$  and  $\rho'$  and their ratios in order to demonstrate CT. For these channels the analysis will be similar to that for  $\rho^0$ , but the rates will be lower due to the smaller production cross sections. The estimates of the required period of data taking and of the target thicknesses are subject of further analysis.

We consider also a possibility to study CT via coherent production of hadron pairs with large relative transverse momenta. The experimental procedure would be similar to that used in the Fermilab experiment E791 [26], in which CT was observed in coherent diffraction of pions into high- $p_t$  di-jets. We will select a sample of events with high- $p_t$  hadron pair and an additional requirement that all observed charged hadrons carry at least 90% of the energy of  $\gamma^*$ . An estimate of  $t$  will be obtained using momenta of all measured charged hadron tracks. The expected resolution in  $t$ , which will be crucial for selection of

the coherent sample, will be determined from a dedicated simulation and reconstruction of events with high- $p_t$  hadron pairs.

Finally we mention few experimental aspects which have to be further investigated.

Here we propose to position the nuclear targets downstream of the polarized target. Then the CT physics could complement the standard COMPASS program by using the downstream nuclear targets simultaneously with the polarized target. Similar target configuration was already used during the 1985 running of the EMC experiment, when the polarized target was used together with several nuclear targets situated downstream of PT.

The effect of the downstream nuclear targets on the hadrons coming from the polarized target should be small. For instance, for the reconstructible tracks of hadrons from PT, only about 4% of slow pions from  $D^*$  decays and about 1% of hadrons from  $D^0$  decays will be in the acceptance of the proposed nuclear target [39]. For the scattered muon coming from PT and passing through the nuclear target, the additional multiple Coulomb scattering should result in a small increase of the errors of the reconstructed position of the event vertex.

Assuming a dedicated run with unpolarized targets, different target configurations for CT studies are possible. With more available space one could envisage targets at least about 4 times thicker than the thin targets presented earlier. Thus the four-fold reduction of the data taking time will be possible. With an even larger amount of available beam time, one could expose more nuclear targets of different materials, and in addition the liquid hydrogen or deuterium targets. The latter ones are also important for measurements of *off-forward parton distributions* (also referred to as *skewed parton distributions* or *generalized parton distributions*) [40]. For a dedicated run with unpolarized targets, one could take advantage of a possibility of adding a recoil detector. This is crucial for certain processes, e.g. Deep Virtual Compton Scattering (DVCS), but in any case it will help to reduce the non-exclusive background for any exclusive process.

## 7 Conclusions

We have simulated and analysed exclusive  $\rho^0$  muoproduction ( $\mu A \rightarrow \mu \rho^0 A$  and  $\mu A \rightarrow \mu \rho^0 N(A-1)$ ) at the COMPASS experiment using thin nuclear targets of carbon and lead. For muon beam energy of 190 GeV and a trigger for medium and large  $Q^2$ , the covered kinematic range is  $2 < Q^2 < 20 \text{ GeV}^2$  and  $35 < \nu < 170 \text{ GeV}$ .

Good resolutions in  $Q^2$ ,  $l_c$ ,  $t$  ( $p_t^2$ ) and  $\cos\theta$  are feasible. An efficient selection of coherent or incoherent events is possible by applying cuts on  $p_t^2$ . In order to obtain the samples of events initiated with a probability of about 80% by either  $\gamma_L^*$  or  $\gamma_T^*$ , the cuts on the  $\rho^0$  decay angular distribution of  $\cos\theta$  will be used. The search for CT could be facilitated by using the events with  $l_c$  values exceeding the sizes of the target nuclei. The fraction of such events is substantial and the covered  $Q^2$  range seems sufficient to observe CT.

We showed high sensitivity of the measured ratio  $R_T$  of nuclear transparencies for lead and carbon for different models of nuclear absorption. Good statistical accuracy of the measured  $R_T$  may be achieved already for one year of data taking. These measurements, taken at different  $Q^2$  intervals, may allow to discriminate between different mechanisms of the interaction of the hadronic components of the virtual photon with the nucleus.

In conclusion, the planned comprehensive studies of exclusive vector meson production on different nuclear targets at the COMPASS experiment should unambiguously demon-



strate CT.

## 8 Acknowledgements

The authors gratefully acknowledge useful discussions with L. Frankfurt. We thank also S. Kananov for discussions on the ZEUS exclusive  $\rho^0$  data. The work was supported in part by the Israel Science Foundation (ISF) founded by the Israel Academy of Sciences and Humanities, Jerusalem, Israel and by the Polish State Committee for Scientific Research (KBN SPUB Nr 621/E-78/SPUB-M/CERN/P-03/DZ 298/2000 and KBN grant Nr 2 P03B 113 19). One of us (A.S.) acknowledges support from the Raymond and Beverly Sackler Visiting Chair in Exact Sciences during his stay at Tel Aviv University.

## References

- [1] F.E. Low, Phys. Rev. **D 12** (1975) 163.
- [2] G. Bertsch *et al*, Phys. Rev. Lett. **47** (1981) 297.
- [3] S.J. Brodsky, L.L. Frankfurt, J.F. Gunion, A.H. Mueller, M.I. Strikman, Phys. Rev. **D 50** (1994) 3134.
- [4] L.L. Frankfurt, G.A. Miller and M.I. Strikman, Phys. Lett. **B304** (1993) 1;  
L.L. Frankfurt, G.A. Miller and M.I. Strikman, Ann. Rev. Nucl. Part. Sci. **45** (1994) 501.
- [5] B. Blättel, G. Baym, L.L. Frankfurt and M.I. Strikman, Phys. Rev. Lett. **70** (1993) 896.
- [6] L.L. Frankfurt, W. Köpf and M.I. Strikman, Phys. Rev. **D54** (1996) 3194.
- [7] L.L. Frankfurt, A.V. Radyushkin and M.I. Strikman, Phys. Rev. **D55** (1997) 98.
- [8] M.D. Sokoloff *et al*, Phys. Rev. Lett. **57** (1986) 3003.
- [9] L.L. Frankfurt, V. Guzey, W. Köpf, M. Sargsian and M.I. Strikman, *Color Transparency and Color Opacity in Coherent Production of Vector Mesons off Light Nuclei at Small x*, hep-ph/9608492.
- [10] L.L. Frankfurt and M.I. Strikman, Phys. Lett. **B382** (1996) 6.
- [11] A.H. Mueller, Proc. of the XVII Rencontre de Moriond, 1982, ed. J. Trân Thanh Vân, Editions Frontières, Gif-sur-Yvette, France, 1982, p.13.
- [12] G. Baum *et al*, *COMPASS, A Proposal for a Common Muon and Proton Apparatus for Structure and Spectroscopy*, CERN/SPSLC/96-14, SPSC/P 297 (1996) and CERN/SPSLC 96-30 (1996), <http://wwwcompass.cern.ch/compass/proposal/welcome.html>.
- [13] F. Bradamante, Prog. Part. Nucl. Phys. **44** (2000) 339.
- [14] T. Renk, G.Piller and W. Weise, *Coherence Effects in Diffractive Electroproduction of  $\rho^0$  Mesons from Nuclei*, hep-ph/0008109, submitted to Nucl. Phys. A.

- [15] HERMES Collab., K. Ackerstaff *et al*, Phys. Rev. Lett. **82** (1999) 3025.
- [16] P.D.B. Collins, *Introduction to Regge theory*, Cambridge Univ. Press, Cambridge, 1977.
- [17] L.L. Frankfurt, M.V. Polyakov and M.I. Strikman,  *$N \rightarrow \Delta$  DVCS, exclusive DIS processes and skewed quark distributions in large  $N_c$  limit*, Workshop on Jefferson Lab. Physics and Instrumentation with 6-12 GeV Beams and Beyond, Newport News, Virginia, June 1998, hep-ph/9808449.
- [18] H1 Collab., C. Adloff *et al*, Eur. Phys. J. **C13** (2000) 371.
- [19] ZEUS Collab., J. Breitweg *et al*, Eur. Phys. J. **C6** (1999) 603.
- [20] L.L. Frankfurt and M.I. Strikman, Eur. Phys. J. **A5** (1999) 293.
- [21] A.S. Carroll *et al*, Phys. Rev. Lett. **61** (1988) 1698.
- [22] N.C.R. Makins *et al*, Phys. Rev. Lett. **72** (1994) 1986;  
T.G. O'Neil *et al*, Phys. Lett. **B351** (1995) 87.
- [23] NMC, P. Amaudruz *et al*, Nucl. Phys. **B371** (1992) 553;  
NMC, M. Arneodo *et al*, Phys. Lett. **B332** (1994) 195.
- [24] E665 Collab., M.R. Adams *et al*, Phys. Rev. Lett. **74** (1995) 1525.
- [25] NMC, M. Arneodo *et al*, Nucl. Phys. **B429** (1994) 503.
- [26] E791 Collab., E.M. Aitala *et al*, Phys. Rev. Lett. **86** (2001) 4773;  
E791 Collab., E.M. Aitala *et al*, Phys. Rev. Lett. **86** (2001) 4768.
- [27] A. Sandacz, *Hard Exclusive Meson Production at COMPASS*, COMPASS Note 2000-1,  
<http://wwwcompass.cern.ch/compass/notes>.
- [28] J. Pochodzalla, L. Mankiewicz, M. Moinester, G. Piller, A. Sandacz, M. Vanderhaeghen, *Exclusive Meson Production at COMPASS*, hep-ph/9909534.
- [29] A. Tripet, presented at the 7th International Workshop on Deep Inelastic Scattering and QCD, Zeuthen, Germany, 19-23 April 1999; Proceedings, J. Blümlein and T. Riemann, Nucl. Phys. B, Proc. Suppl. **79** (1999) 529.
- [30] NMC, P. Amaudruz *et al*, Z. Phys. **C54** (1992) 239.
- [31] K. Kurek, *QED Radiative Corrections in Exclusive  $\rho^0$  Leptoproduction*, DESY-96-209,  
hep-ph/9609240.
- [32] K. Schilling and G. Wolf, Nucl. Phys. **B61** (1973) 381.
- [33] D. Schildknecht, G.A. Schuler and B. Surrów, Phys. Lett. **B449** (1999) 328.
- [34] J.D. Jackson, Nuovo Cimento **34** (1964) 1644.
- [35] K.S. Kölbig and B. Margolis, Nucl. Phys. **B6** (1968) 85.
- [36] T.H. Bauer *et al*, Rev. Mod. Phys. **50** (1978) 261;  
J. Ballam *et al*, Phys. Rev. **D5** (1972) 545;  
P. Joos *et al*, Nucl. Phys. **B113** (1976) 53.

- [37] ZEUS Collab., J. Breitweg *et al*, Eur. Phys. J. **C12** (2000) 393.
- [38] H. de Vries *et al*, Atomic Data and Nucl. Data Tables **36** (1987) 495.
- [39] A. Mielech (COMPASS), private communication.
- [40] X. Ji, Phys. Rev. Lett. **78** (1997) 610; Phys. Rev. **D 55** (1997) 7114;  
A.V. Radyushkin, Phys. Lett. **B380** (1996) 417; Phys. Rev. **D 56** (1997) 5524;  
J.C. Collins, L. Frankfurt and M. Strikman, Phys. Rev. **D 56** (1997) 2982.

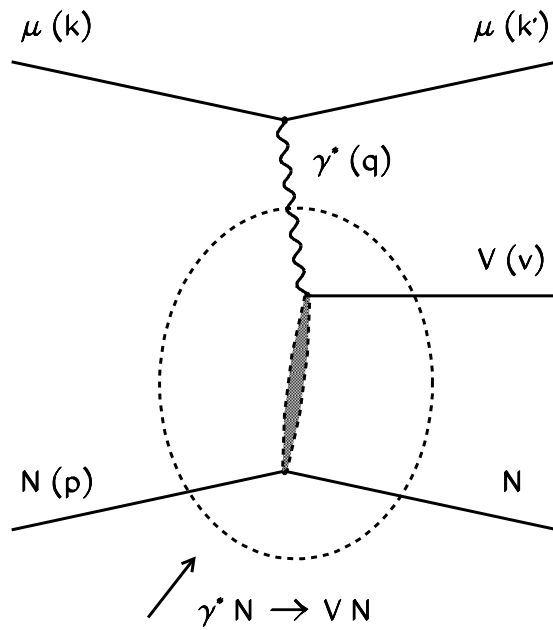


Figure 1: Diagram of exclusive meson muoproduction  $\mu N \rightarrow \mu N V$ , where meson  $V$  is the only produced particle. Corresponding four-momenta are indicated in brackets (cf. Table 1) .

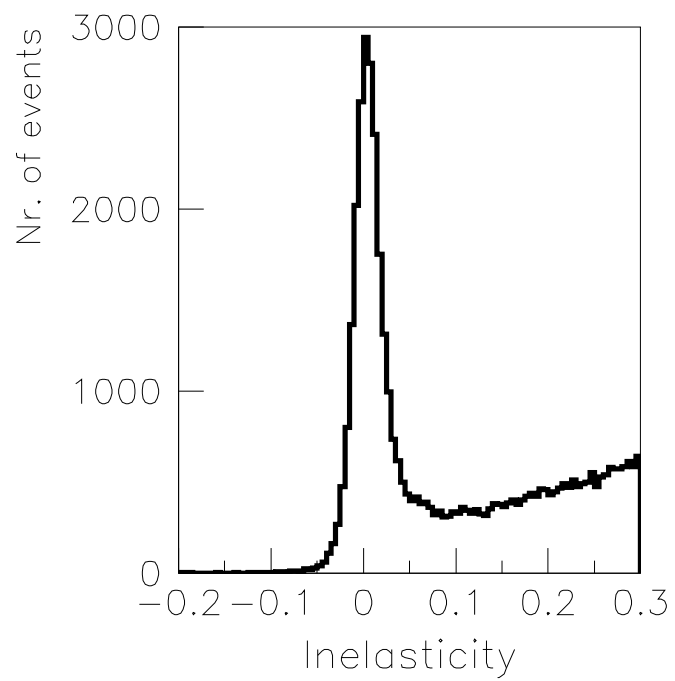


Figure 2: Inelasticity distribution. The SMC preliminary results [29] for  $\mu N \rightarrow \mu \rho^0 N$ .

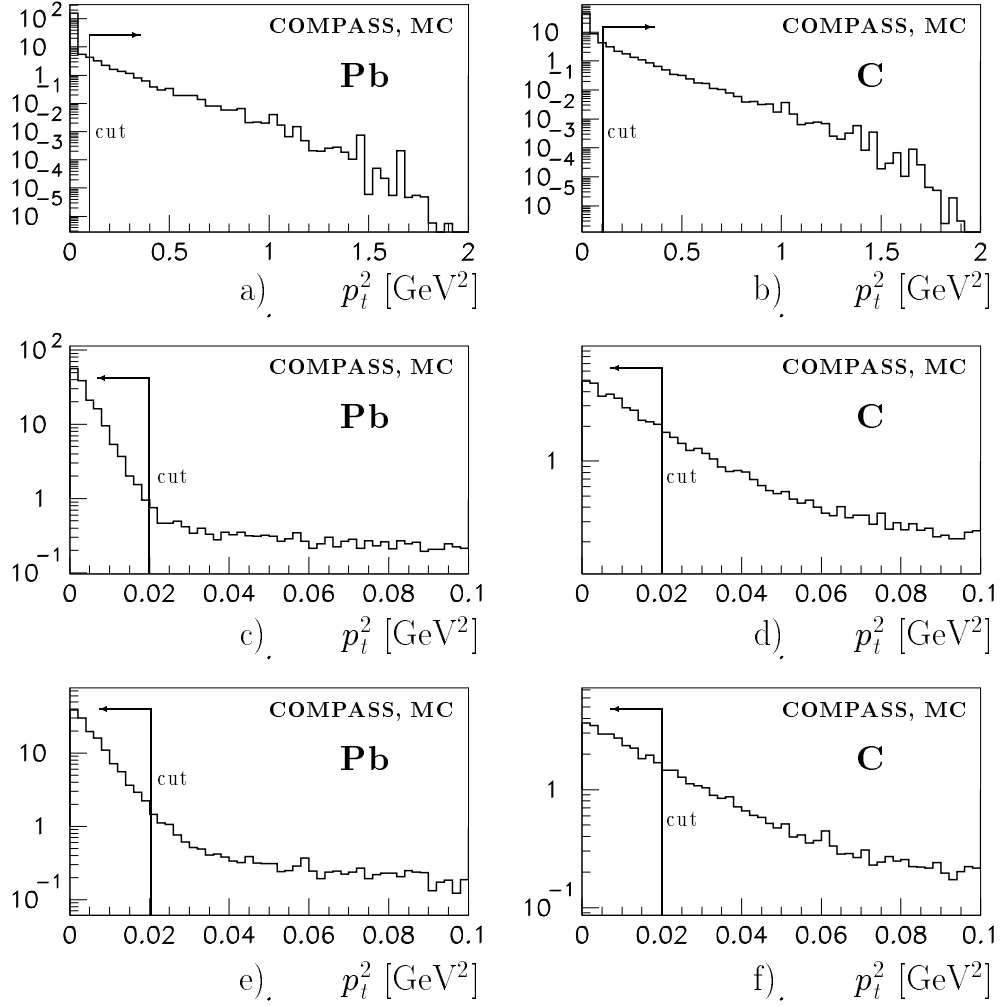


Figure 3: Distributions of  $p_t^2$  for the lead (left) and carbon (right) targets. The distributions a) and b) at the top are for the generated events and the wide range of  $p_t^2$ , whereas those in the middle, c) and d), correspond to the range of low  $p_t^2$ . The bottom distributions, e) and f), are for the accepted events, with the kinematical smearing taken into account. The arrows show the cuts described in the text.

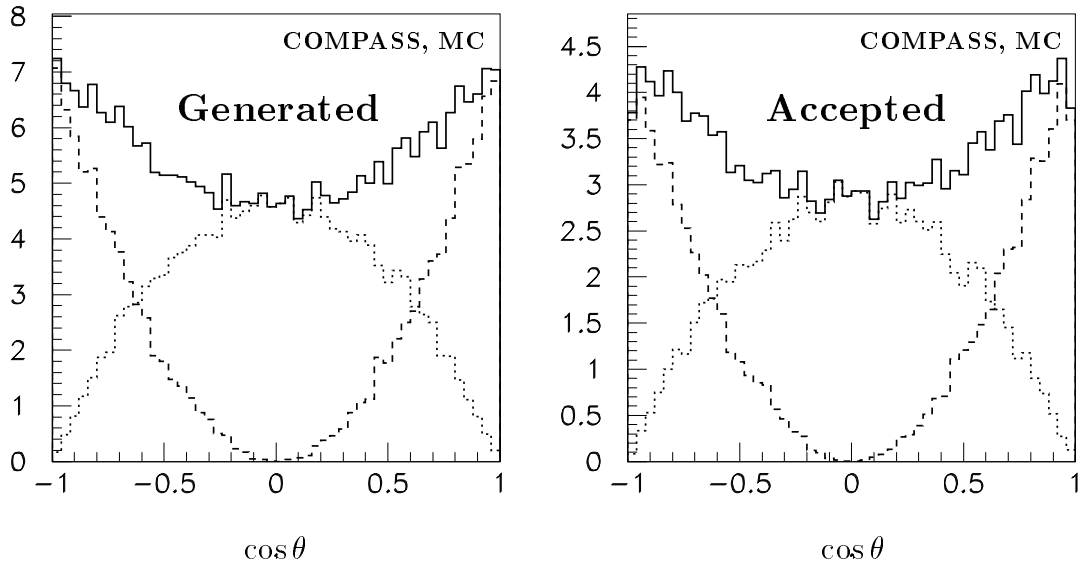


Figure 4: Distributions of  $\cos\theta$  for the pions ( $\pi^+$ ) from the decays of  $\rho^0$  mesons produced on lead, for generated (left) and accepted (right) events. For the latter ones the effects of the kinematical smearing were taken into account. The dashed- and dotted-line histograms are for the longitudinally and transversely polarized  $\rho^0$ 's, respectively, and the solid-line histograms are for their sum.

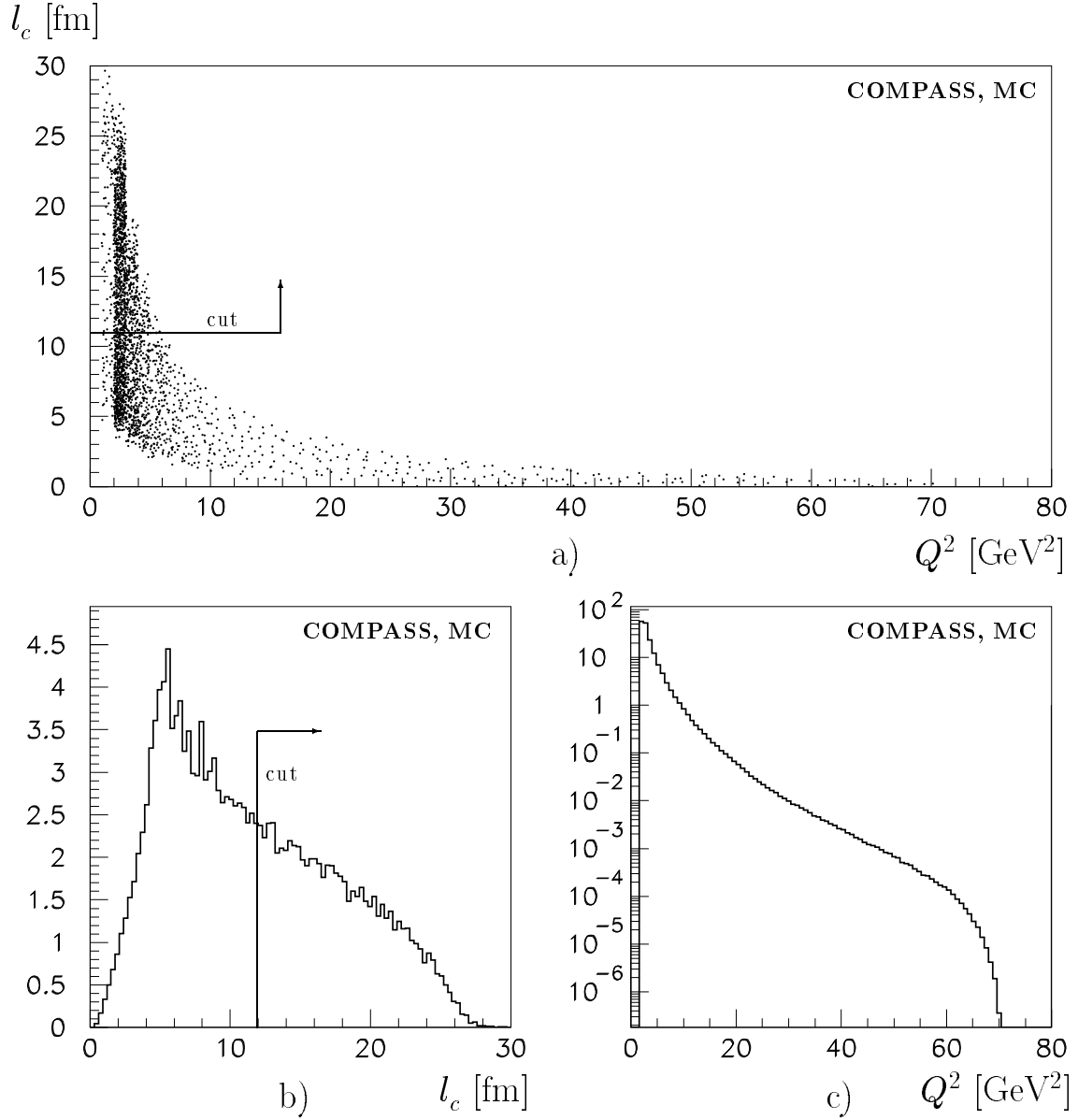
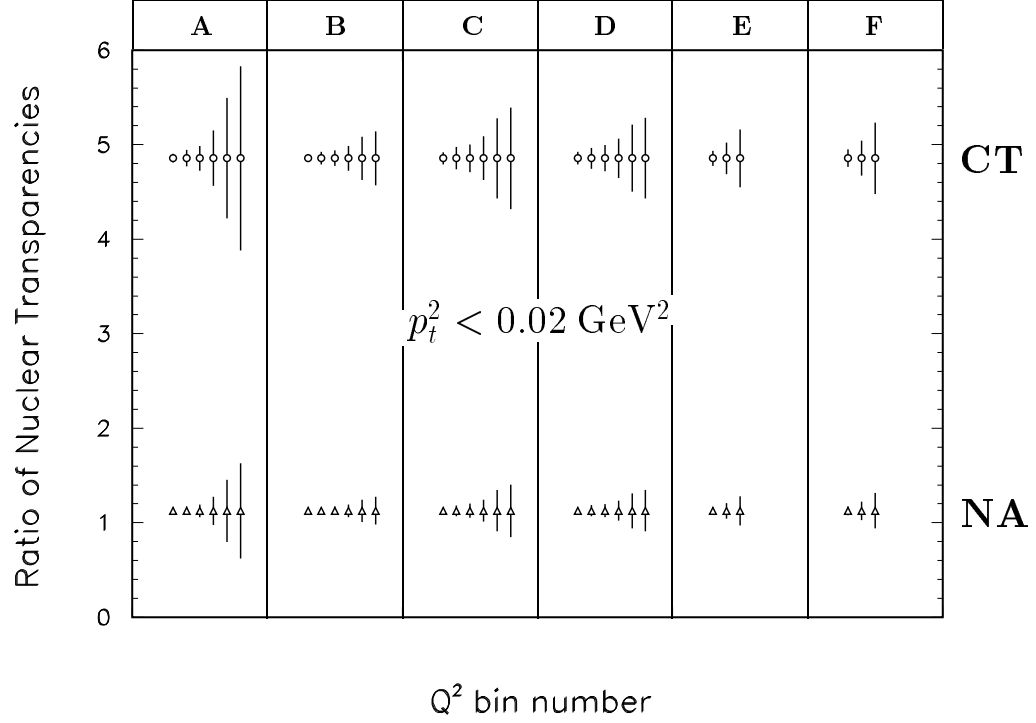


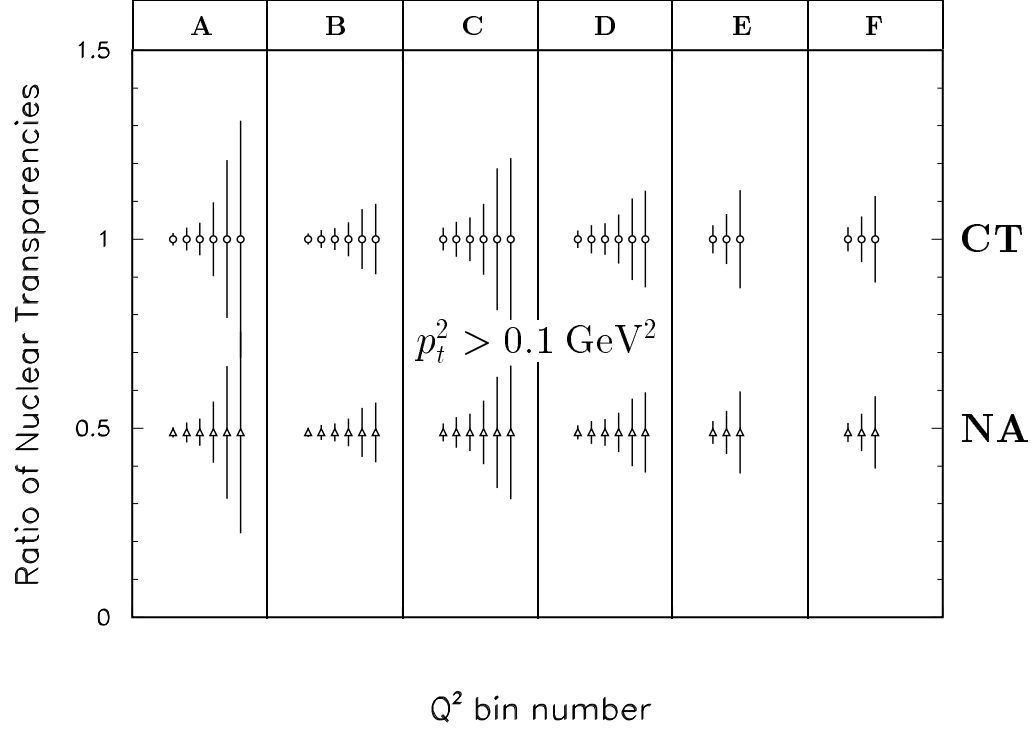
Figure 5: Correlation of  $l_c$  and  $Q^2$ . The plot a) and its projections b) and c) were obtained for the accepted events from  $\rho^0$  production on lead. The arrows show the cut discussed in the text.





set	conditions
<b>A</b>	MT
<b>B</b>	FT
<b>C</b>	FT + $ \cos\theta  < 0.4$
<b>D</b>	FT + $ \cos\theta  > 0.7$
<b>E</b>	FT + $ \cos\theta  < 0.4$ + $l_c > 11$ fm
<b>F</b>	FT + $ \cos\theta  > 0.7$ + $l_c > 11$ fm

Figure 6: Expected statistical precision of the measurement of the ratio  $R_T$  of nuclear transparencies for lead and carbon for  $p_t^2 < 0.02$  GeV<sup>2</sup> and for different  $Q^2$  bins, for CT (upper band) and for NA (lower band) models. The  $Q^2$  bins are defined in Table 3. Sets A, B, C, D, E and F correspond to the conditions specified in the table below the plot.



set	conditions
<b>A</b>	MT
<b>B</b>	FT
<b>C</b>	FT + $ \cos \theta  < 0.4$
<b>D</b>	FT + $ \cos \theta  > 0.7$
<b>E</b>	FT + $ \cos \theta  < 0.4$ + $l_c > 11$ fm
<b>F</b>	FT + $ \cos \theta  > 0.7$ + $l_c > 11$ fm

Figure 7: Expected statistical precision of the measurement of the ratio  $R_T$  of nuclear transparencies for lead and carbon for  $p_t^2 > 0.1 \text{ GeV}^2$  and for different  $Q^2$  bins, for CT (upper band) and for NA (lower band) models. The  $Q^2$  bins are defined in Table 3. Sets A, B, C, D, E and F correspond to the conditions specified in the table below the plot.